Title

Electronic structure of correlated topological insulator candidate YbB6 studied by photoemission and quantum oscillation

Journal

Chinese Physics B, 29(1)

ISSN

1674-1056

Authors

Zhang, T

Li, G

Sun, SC

et al.

Publication Date

2020

DOI

10.1088/1674-1056/ab6206

Peer reviewed

SPECIAL TOPIC — Topological semimetals

Electronic structure of correlated topological insulator candidate YbB_6 studied by photoemission and quantum oscillation

T Zhang(张腾)[1], G Li(李岗)[2,3], S C Sun(孙淑翠)[1], N Qin(秦娜)[1], L Kang(康璐)[1], S H Yao(姚淑华)[4], H M Weng(翁红明)[3,5,6,7,8], S K Mo[9], L Li(李璐)[2], Z K Liu(柳仲楷)[10,11], L X Yang(杨乐仙)[1,12], and Y L Chen(陈宇林)[1,10,11,13,†]

[1] *State Key Laboratory of Low Dimensional Quantum Physics, Department of Physics, Tsinghua University, Beijing* 100084, *China*
[2] *Department of Physics, University of Michigan, Ann Arbor, MI* 48109, *USA*
[3] *Beijing National Laboratory for Condensed Matter Physics and Institute of Physics, Chinese Academy of Sciences, Beijing* 100190, *China*
[4] *National Laboratory of Solid State Microstructures & Department of Materials Science and Engineering, Nanjing University, Nanjing* 210093, *China*
[5] *Collaborative Innovation Center of Quantum Matter, Beijing, China*
[6] *Songshan Lake Materials Laboratory, Dongguan* 523808, *China*
[7] *CAS Center for Excellence in Topological Quantum Computation, Beijing* 100190, *China*
[8] *Physical Science Laboratory, Huairou National Comprehensive Science Center, Beijing* 101400, *China*
[9] *Advanced Light Source, Lawrence Berkeley National Laboratory, Berkeley, CA* 94720, *USA*
[10] *School of Physical Science and Technology, ShanghaiTech University and CAS-Shanghai Science Research Center, Shanghai* 201210, *China*
[11] *ShanghaiTech Laboratory for Topological Physics, Shanghai* 200031, *China*
[12] *Frontier Science Center for Quantum Information, Beijing* 100084, *China*
[13] *Department of Physics, Clarendon Laboratory, University of Oxford Parks Road, Oxford OX*1 3*PU, UK*

(Received 22 November 2019; revised manuscript received 9 December 2019; accepted manuscript online 16 December 2019)

Angle-resolved photoemission spectroscopy (ARPES) and torque magnetometry (TM) measurements have been carried out to study the electronic structures of a correlated topological insulator (TI) candidate YbB_6. We observed clear surface states on the [001] surface centered at the $\bar{\Gamma}$ and $\bar{M}$ points of the surface Brillouin zone. Interestingly, the fermiology revealed by the quantum oscillation of TM measurements agrees excellently with ARPES measurements. Moreover, the band structures we observed suggest that the band inversion in YbB_6 happens between the Yb_{5d} and B_{2p} bands, instead of the Yb_{5d} and Yb_{4f} bands as suggested by previous theoretical investigation, which will help settle the heavy debate regarding the topological nature of samarium/ytterbium hexaborides.

Keywords: topological insulator, electronic structure, surface states

PACS: 73.20.At, 73.20.–r, 71.27.+a **DOI:** 10.1088/1674-1056/ab6206

1. Introduction

Topological insulators (TIs) represent a new class of materials intensively studied recently.[1,2] Up to date, most research in the field has been focused on band insulators with weak electron–electron interaction, such as typical V_2–VI_3 (e.g., Bi_2Te_3, Bi_2Se_3, Sb_2Te_3) series[3,4] and III–V–VI_2 ($TlBiTe_2$ and $TlBiSe_2$) series[5,6] compounds, in which the Dirac surface states stem as a result of the s–p band inversion.[1,7] After these initial achievements, the search for TIs in correlated electron systems[8] has attracted increasing research attention, as correlated TIs not only provide a new platform that bridges the topological non-trivial states and other exotic phenomena in correlated materials (such as the formation of the topological Mott insulator[9,10] and topological crystalline insulator[11]), but also provide a test ground to check the theoretical calculation, which has been mostly successful in predicting the weakly interacting TIs.[1,2,7]

Recently, several rare-earth hexaboride compounds have been predicted to be correlated TIs or topological Kondo insulators (TKI), including SmB_6 and YbB_6.[12,13] However, despite the intensive experimental effects on SmB_6 recently,[14–18] the symbolic Dirac fermions formed by the surface state band (SSB) have not been well resolved in SmB_6 as in previously discovered TIs.[1–8] In addition, although the transport measurements show evidence of dominating surface channels at low temperature, the fermiology extracted from the quantum oscillation of the dHvA effect[19] does not match the Fermi pockets observed by angle-resolved photoemission spectroscopy (ARPES). The lack of SdH oscillation observation further makes the situation puzzling given the high quality of the SmB_6 samples.[20] Moreover, there have been heavy debates about whether SmB_6 is a TKI or trivial insulator. While previous ARPES measurement suggested topological surface states with helical spin structure, a recent ARPES study provided a topologically trivial explanation for the observed band

†Corresponding author. E-mail: yulin.chen@physics.ox.ac.uk

structure of SmB_6.[21]

Under this circumstance, YbB_6 receives focused interest recently. Although similar to SmB_6, the electron correlation in YbB_6 is relatively weak,[22] it can serve as an ideal model system to investigate the topologically non-trivial states in correlated electron system: on one hand, the interaction effect in YbB_6 is weaker than that in SmB_6, thus the electronic structure can be understood relatively easily; on the other hand, the interaction in YbB_6 is already strong enough thus the previous theoretical calculation[12] has shown obvious deviation from the ARPES experimental observation. On the other hand, similar to the situation in SmB_6, there have been heavy debates regarding the topological nature of YbB_6.[22–25] It is thus necessary to further study the electronic structure of this TKI candidate.

In this work, we studied the electronic structure of YbB_6 by both ARPES and torque magnetometry (TM) methods. We directly observed the SSB in YbB_6. Interestingly, the fermiology revealed by the quantum oscillation of TM measurements shows excellent agreement with the ARPES results. Moreover, the band structure we observed suggests that the band inversion in YbB_6 happens between the Yb_{5d} and B_{2p} bands — different from the previous calculation[12] that suggested an inversion between the Yb_{5d} and Yb_{4f} bands. This difference clearly shows the effect of strong electron–electron interaction and the importance of experimental studies in correlated TI materials. With the input from our experiments, we were able to correct the previous theoretical calculation,[12] paving a way to develop proper theoretical methods for exploring other strongly correlated TI materials.

2. Experiment methods

2.1. Sample growth

High quality single crystals of YbB_6 were grown by spontaneous nucleation technique from high temperature solutions, using Al as the solvent. The starting materials are Yb, B, and Al with a purity of 99.99%. The molar ratio of solute to solvent is 1 : 10. The mixture was heated to 1500 °C and held at this temperature for 24 h to homogenize the solution in an argon atmosphere. After superheating, the melt was cooled to 1450 °C quickly and then slowly to 700 °C. After this, the melt was cooled to room temperature naturally. Single crystals with sizes up to 4 mm×0.8 mm×0.4 mm were obtained by dissolving the Al flux with hydrochloric acid.

2.2. ARPES measurements

ARPES measurements were performed at beamline 10.0.1 of Advanced Light Source (ALS) at Lawrence Berkeley National Laboratory and beamline 5.4 of Stanford Synchrotron Radiation Lightsource (SSRL). Single crystal samples of YbB_6 were cleaved *in situ* and flat shiny surfaces could be obtained along the (001) plane. In both facilities, the measurement pressure was kept better than 3×10^{-11} Torr, and data were recorded by Scienta R4000 electron analyzers at 5 K/15 K sample temperatures at SSRL/ALS. The total convolved energy and angle resolutions were 9/25 meV and 0.2°/0.2° at SSRL/ALS, respectively. The sample surface was monitored continually by measuring the reference valence spectra. All the spectra reported here were measured within 18 hours of cleavage.

2.3. Torque magnetometry

The magnetization measurements were carried out with a home-built cantilever-based torque magnetometry apparatus at University of Michigan as well as in the National High Magnetometry Laboratory. Cantilevers were made from thin brass foils. We deposited a gold film on a sapphire chip and put it under the cantilever. The torque was tracked by measuring the capacitance between the cantilever and the gold film, using an AH2700 A capacitance bridge. To calibrate the spring constant of the cantilever, we rotated the cantilever setup under zero magnetic field to measure the capacitance change caused by the weight of the sample itself.[26]

3. Results and discussion

The crystal structure of YbB_6 is shown in Fig. 1(a), where Yb forms a cubic lattice with a B_6-octahedron residing inside each unit. The Brillouin zone (BZ) is illustrated in Fig. 1(b) with high symmetry points labeled. The high quality of the samples is illustrated by the Laue characterization [Fig. 1(c)] and the powder x-ray diffraction [Fig. 1(d)]. Figure 1(e) illustrates the characteristic Yb_{5p} and Yb_{4f} core levels.

The Fermi surface (FS) map of YbB_6 in Fig. 1(f) shows two sets of distinct FS pockets at the $\bar{\Gamma}$ and $\bar{X}$ points, respectively: a large circular hollow pocket (FS area ~ 0.04 Å^{-2}) at $\bar{\Gamma}$ and an elliptical hollow pocket (FS area ~ 0.06 Å^{-2}) centered at $\bar{X}$, each enclosing a smaller filled disk-like pocket inside. To check the nature of these FS pockets, we focus our measurements on each pocket and perform the photon-energy dependent ARPES measurements. In Fig. 1(g), the evolution of the FS pockets at both $\bar{\Gamma}$ and $\bar{X}$ is illustrated, which shows distinct behaviors of the outer hollow FS pockets and the inner disk-like pockets – while the outer hollow pockets centered at both $\bar{\Gamma}$ and $\bar{X}$ do not change their shape with photon energy, the inner disk-like pockets change dramatically with photon energy – indicating the 3-dimensional (3D) and 2-dimensional (2D) nature of the inner disk-like feature and out hollow pockets.

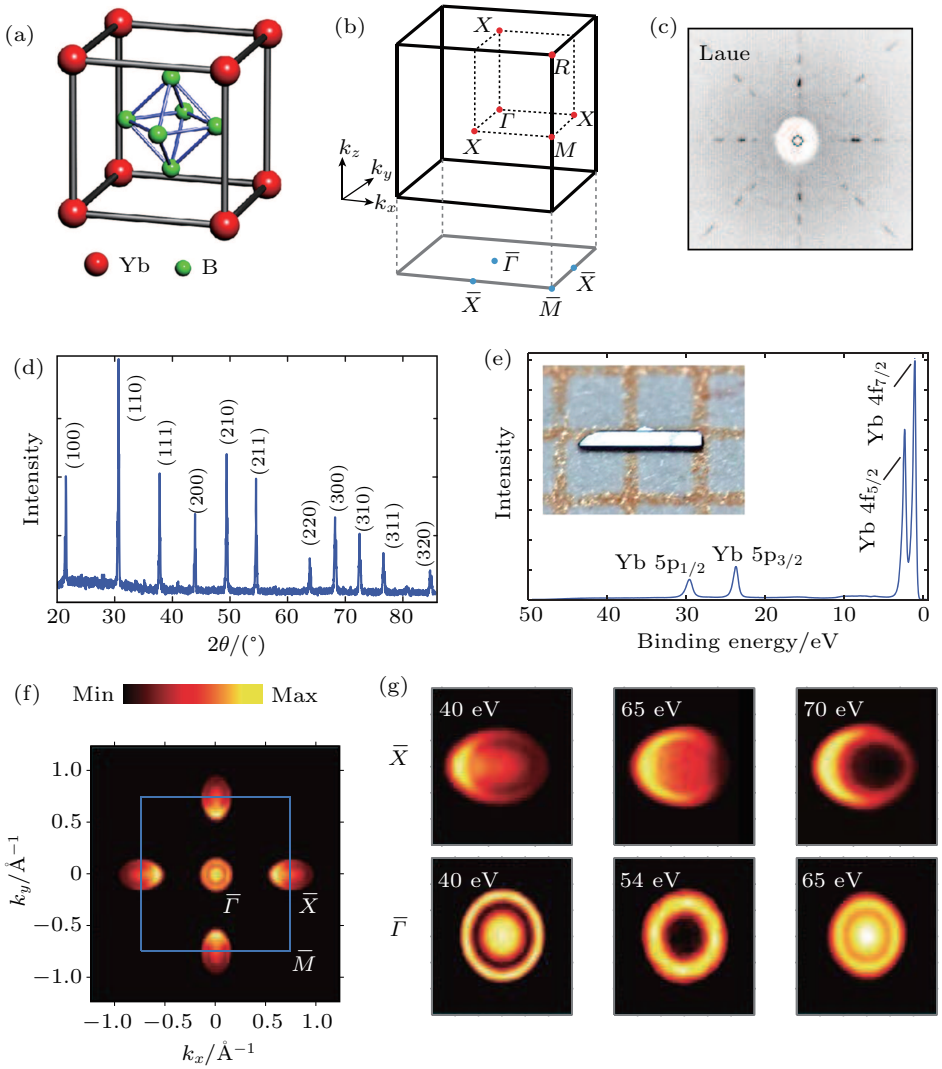

Fig. 1. An overview of YbB_6. (a) Crystal structure of YbB_6. (b) The 3D and surface projected 2D Brillouin zones of YbB_6, red and cyan dots indicate the high-symmetry points. (c) and (d) Laue pattern and powder x-ray diffraction showing the high quality of the crystals. (e) Core level photoemission spectrum showing the prominent 4f- and 5p-electron characteristic peaks of Yb. The inset in (f) shows a flat sample surface along (001) direction. (f) Fermi surface of YbB_6 in the first BZ obtained by integrating ARPES intensity in an energy window of 20 meV around E_F. The blue lines indicate the projected surface BZ. (g) Zoom-in plots of FS maps measured using different photon energies at both $\bar{\Gamma}$ and $\bar{X}$.

This difference in the dimensionality of the FS pockets can also be seen from the band dispersions. The band structure related to the FSs around $\bar{\Gamma}$ is illustrated in Figs. 2(a)–2(c), where the 3D electronic structure and the band dispersion along the $\bar{X}$–$\bar{\Gamma}$–$\bar{X}$ high symmetry direction are shown in Figs. 2(a) and 2(b), respectively. Around $\bar{\Gamma}$, there are sharp linear bands outside some fluffy bands, which can be clearly resolved in the momentum distribution curves (MDCs) in Fig. 2(c). This distinction between the dispersion sharpness comes from the different dimensionality of the bands: due to the k_z broadening,[27] the 3D bands that have strong k_z-dispersion will smear up in the ARPES measurement, while the 2D bands do not suffer from such broadening and remain sharp. To further verify this, we show the broad range (40–90 eV) photon energy dependent measurements in Fig. 2(d). Indeed, the MDC peaks of the outer band form two straight lines, indicating no k_z-dispersion, or the 2D (surface) nature of the outside band. On the other hand, the inner pocket shows dramatic variation at different photon energies, confirming its bulk nature. The similar measurements near the $\bar{X}$ points are shown in Figs. 2(e)–2(h) and the same conclusion can be drawn that the outer band originates from the surface and the inner one shows clearly the bulk character.

To examine the origin of the SSBs in YbB_6, we compare our observed band structure and the previous theoretical work,[12] and discover a couple of clear discrepancies. In the previous *ab initio* calculation, the topological surface state originated from the band inversion between Yb_{5d} and Yb_{4f} as schematically illustrated in Fig. 3(a), thus the SSBs should emerge at the inversion band gap between the Yb_{5d} and Yb_{4f} bands and are very close to the flat 4f bands which were predicted to reside near the E_F.[12] However, our measurements in a broad energy range do not show the Yb_{5d} band that hybridizes with the flat Yb_{4f} band. Actually, the SSBs near E_F are well separated from the Yb_{4f} band that resides about 1 eV below E_F [Figs. 3(c) and 3(d)]. These discrepancies suggest

that the previous calculation may not have accounted for the electron correlation effect accurately and thus needs to be improved. It is interesting to note that the electronic structure and the origin of the surface state in SmB_6 are in strike contrast to those in YbB_6, although they share a common crystal structure. In SmB_6, the f orbital locates close to the Fermi level so that it can hybridize with the dispersive d orbital to induce a band inversion. The surface states emerge in the inverted band gap between the f and d orbitals, consistent with the mechanism shown in Fig. 3(a).

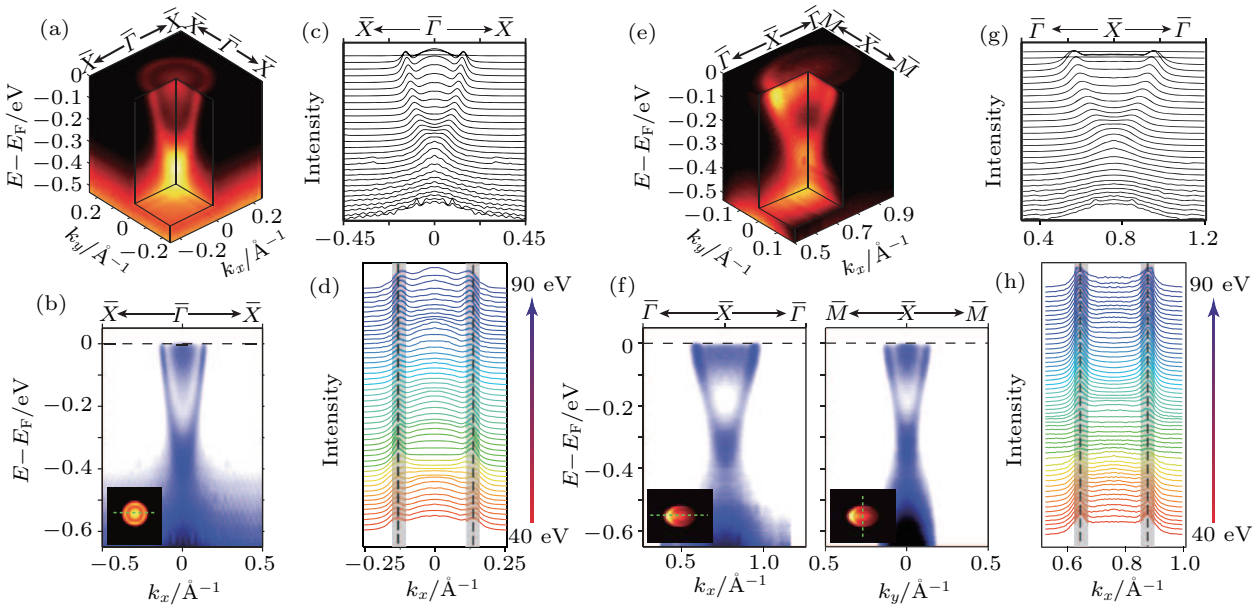

Fig. 2. Electronic structure of YbB_6 and identification of the surface states. (a) 3D illustration of the band structure of YbB_6 around the $\bar{\Gamma}$ point measured with photon energy $h\nu = 65$ eV. (b) Photoemission intensity plot along $\bar{X}$–$\bar{\Gamma}$–$\bar{X}$. The inset shows the direction of the cut. (c) Stacked plot of MDCs from the cut in panel (b). (d) Photon energy dependence of MDCs at E_F along $\bar{X}$–$\bar{\Gamma}$–$\bar{X}$, confirming the weak k_z dispersion of the band around $\bar{\Gamma}$. (e) 3D illustration of the band structure of YbB_6 around the $\bar{X}$ point measured with photon energy $h\nu = 40$ eV. (f) Photoemission intensity plots along $\bar{\Gamma}$–$\bar{X}$–$\bar{\Gamma}$ (left) and along $\bar{M}$–$\bar{X}$–$\bar{M}$ (right). The insets show the direction of the cuts. (g) Stacked plot of MDCs from the cut in the left panel of (f). (h) Photon energy dependence of MDCs at E_F along $\bar{\Gamma}$–$\bar{X}$–$\bar{\Gamma}$, confirming the weak k_z dispersion of the band around $\bar{X}$.

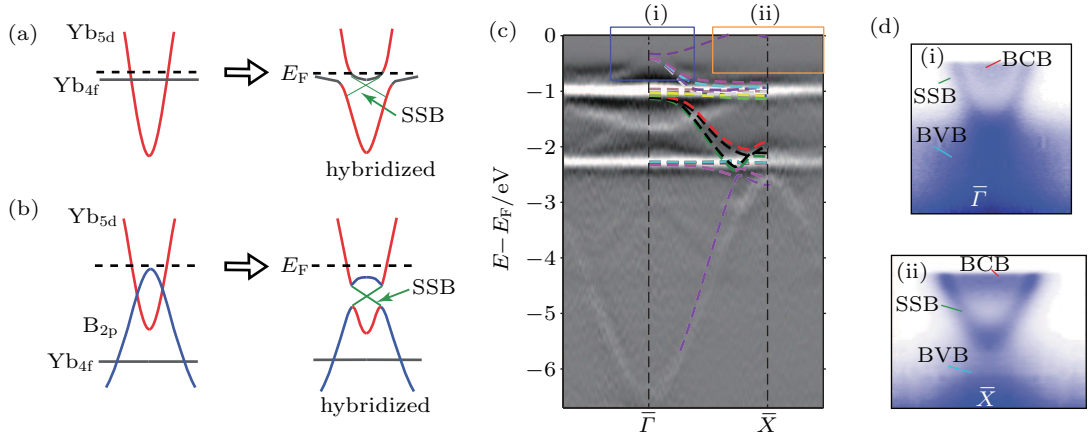

Fig. 3. The origin of the surface states. (a) Schematic of the scenario proposed in Ref. [12], where the band inversion and inverted band gap take place between the Yb_{4f} and Yb_{5d} bands. (b) Schematic of the scenario where the band inversion and inverted band gap take place between the Yb_{5d} and B_{2p} bands. (c) Wide range photoemission intensity plot along $\bar{X}$–$\bar{\Gamma}$–$\bar{X}$. Curves on top show the *ab initio* calculation results with on-site Coulomb repulsion energy $U = 8$ eV. SSB: surface state band. (d) Zoom-in plots of ARPES spectra in the blue and orange rectangles in panel (c).

To reproduce the experiment results, we carry out further *ab initio* calculation, and find that with much increased on-site Coulomb repulsion energy U (up to 8 eV) compared to the previous study,[12] we are able to reproduce the experimental results and get excellent match. The band inversion now occurs between the B_{2p} and Yb_{5d} bands [Fig. 3(b)], instead of the Yb_{5d} and Yb_{4f} bands [Fig. 3(a)] in the previous calculation.[12] The much lowered Yb_{4f} bands now agree well with the experiments [Fig. 3(c)], and the overall band dispersions also match better with the measurements. We note that a similar result was reported in the same material, except that a much smaller on-site Coulomb repulsion energy U about 4 eV was used.[24]

The experimentally observed bands and FSs are in good consistency with our *ab initio* calculation – the schematic of

the calculated 3D FS is illustrated in Fig. 4(a) (top panel), which consists of two cylindrical surface state FSs (red color) centered at the $\bar{\Gamma}$ and $\bar{X}$ points and an elliptical FS pocket (yellow color) centered at each X point (at the face center of the BZ). In the middle panel, we show the projection of the 3D FS onto the k_x–k_y plane, which agrees excellently with the experimental results (bottom panel).

Given the general discrepancy between the ARPES results and the transport measurements in another correlated TI candidate SmB_6, we would like to check if the fermiology measured by quantum oscillation can be consistent with ARPES in YbB_6. We performed torque magnetometry measurements with the magnetic field close to the crystal (001) axis.[26] The magnetic field tilt angle ϕ is about 0.5° [Fig. 4(b)]. The results are summarized in Fig. 4. The torque measurements reveal clear quantum oscillation in magnetization (the de Hass–van Alphen effect, or dHvA effect). Two major frequencies are observed: $F_\alpha = 400$ T and $F_\beta = 580$ T [Figs. 4(b)–4(d)]. These oscillations arise from the Landau level quantization and the oscillation frequencies are related to the FS area A via the Onsager relation $F = \frac{\Phi_0}{2\pi^2}A$, where $\Phi_0 = 2.07 \cdot 10^{-15}$ T·m^2 is the flux quantum. Thus the corresponding FS volume is determined to be $A_\alpha = 3.8 \times 10^{-2}$ Å^{-2} and $A_\beta = 5.5 \times 10^{-2}$ Å^{-2}. These values are in good agreement with the surface state FS pockets around $\bar{\Gamma}$ [$A_{\bar{\Gamma}} = (4.37 \pm 0.5) \times 10^{-2}$ Å^{-2}] and $\bar{X}$ [$A_{\bar{X}} = (6.41 \pm 0.8) \times 10^{-2}$ Å^{-2}] observed in the ARPES [see the dashed circle and oval in the inset of Fig. 4(d)]. The slight FS area difference between the dHvA and ARPES may result from their different measurement conditions.

We note that figure 4(d) does not reveal the frequency corresponding to the smaller bulk FS (the inner pockets around $\bar{\Gamma}$ and $\bar{X}$), this may be due to the smaller mobility of the bulk electrons (as compared to the surface states). The much smaller Fourier transform (FFT) peak amplitude of the β pocket than that of the α pocket [Fig. 4(d)] may result from the much larger scattering between the surface and bulk electrons at the $\bar{X}$ point. Indeed, as can be seen in the inset of Fig. 4(d), the inner and outer FSs around the $\bar{X}$ point overlap much more than those around the $\bar{\Gamma}$ point.

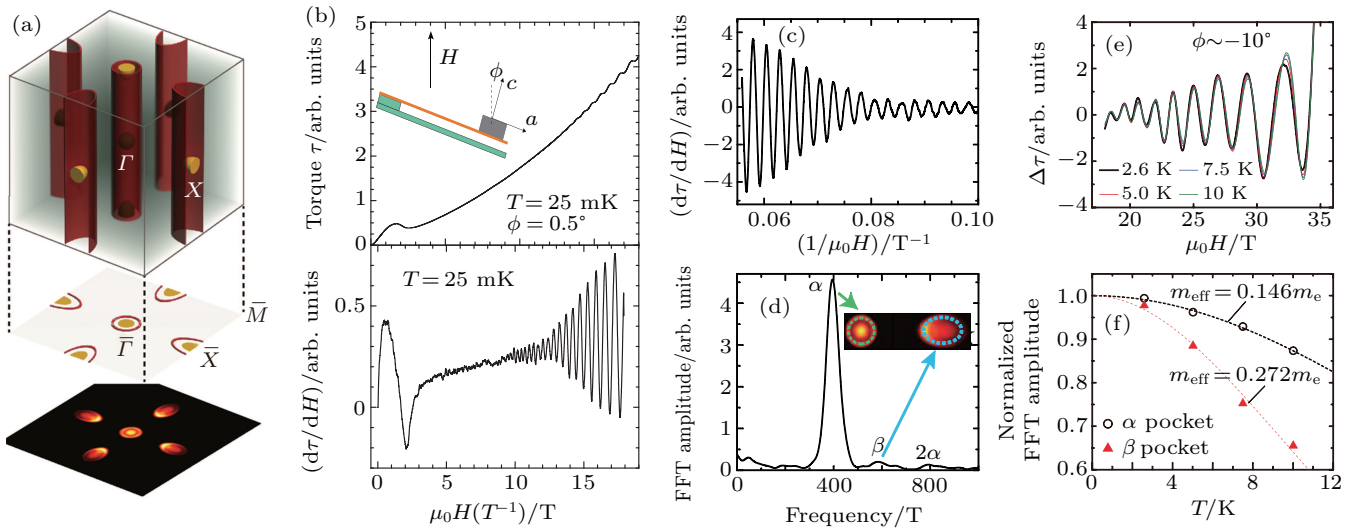

Fig. 4. Magnetoresistance and dHvA oscillations in YbB_6. (a) Illustration of the electronic structure of YbB_6 in the 3D and 2D projected Brillouin zones. The bottom shows the FS obtained in our ARPES experiment. (b) The field dependence magnetic torque τ (upper panel) and its first derivative $d\tau/dH$ (lower panel) of YbB_6. Oscillating patterns are observed in magnetic field higher than 8 T. The inset is the sketch of the experimental setup. The sample stage is rotated to tilt magnetic field H in the crystalline a–c plane. The magnetic field is applied to the sample with a tilt angle ϕ relative to the crystalline c axis. (c) The oscillatory magnetic torques plotted as a function of $1/\mu_0 H$, clearly revealing the quantum oscillation pattern. (d) The main oscillation peak and its harmonic are observed in the FFT transformations of the derivative $d\tau/dH$. The inset shows the corresponding FS pockets of each main oscillation peak, with the extracted area contour of the surface states at $\bar{\Gamma}$ and $\bar{X}$ labeled by the dotted green and blue curves, respectively. (e) The oscillatory torque signals measured at selected temperatures in magnetic field up to 35 T and tilt angle $\phi \sim 10°$. (f) The temperature dependence of the normalized FFT peak amplitudes for both pockets α and β. The effective mass is determined by fitting the temperature dependence to the thermal damping factor R_T of the LK formula.

We further explored the temperature dependence of the dHvA oscillation amplitude. Figure 4(e) shows the oscillatory torque signal at temperature up to 10 K in magnetic field up to 35 T. The overall oscillation amplitude decreases with increasing temperature. It is described by the thermal damping factor in the Lifshitz–Kosovich (LK) formula $R_T = \frac{\alpha T m^*}{B \sinh(\alpha T m^*/B)}$, where the carrier effective mass is $m^* m_e$, m_e is the bare electron mass, and $\alpha = 2\pi^2 k_B m_e / e\hbar = 14.69$ T/K. Figure 4(f) shows the normalized FFT amplitudes of the oscillating frequencies and the fitting based on the R_T factor of the LK formula. The effective mass of pocket α is about $0.15 m_e$ and that of pocket β is about $0.27 m_e$. Based on the oscillation frequency and assuming the corresponding FS is of circular shape, we infer that the Fermi velocity of pocket α is $v_F^\alpha = 8.67 \times 10^5$ m/s $= 5.71$ eV·Å, and that of pocket β is $v_F^\beta = 5.69 \times 10^5$ m/s $= 3.74$ eV·Å, also showing excellent agreement with the velocity data extracted from the ARPES experiment (5.6 eV·Å or 8.5×10^5 m/s for the α pocket and

3.8 eV·Å or 5.76×10^5 m/s for the β pocket along the $\bar{X}\bar{M}$ axis) through linear fitting of the E_F vicinity electrons.

4. Conclusion

In summary, we have observed two sets of FSs by high resolution ARPES measurements in YbB_6 and acquired corresponding dHvA quantum oscillation for the surface part of the $\bar{\Gamma}$ pocket. Our ARPES results help to improve the theoretical understanding regarding the mechanism of the gap opening of the inverted bulk bands and the origin of the surface states in YbB_6. Moreover, the discrepancy between the experiment and the previous theoretical calculation not only shows the vital importance of the experimental effect in the field, but also suggests that the theoretical calculation in correlated materials must be carried out with much caution, unlike in the weakly correlated TIs.

Acknowledgements

This work was supported by the National Natural Science Foundation of China (Grant Nos. 11774190, 11674229, 11634009, and 11774427), the National Key R&D Program of China (Grant Nos. 2017YFA0304600 and 2017YFA0305400). Y. L. C acknowledges the support from the EPSRC (UK) grant EP/K04074X/1 and a DARPA (US) MESO project (No. N66001-11-1-4105). The work at Michigan is mainly supported by the Office of Naval Research through the National Science Foundation under Award No. DMR-1707620 (magnetization measurement). The Advanced Light Source is supported by the Office of Basic Energy Sciences of the U.S. Department of Energy (DE-AC02-05CH11231). The work at SIMES and SLAC National Accelerator Laboratory is supported by the Office of Basic Energy Sciences of the U.S. Department of Energy (DE-AC02-76SF00515). The work at Nanjing University is supported by the National Basic Research Program of China (Grant No. 51002074) and the National Basic Research of China (Grant Nos. 2012CB921503 and 2012CB632702).

References

[1] Qi X L and Zhang S C 2011 *Rev. Mod. Phys.* **83** 1057
[2] Hasan M Z and Kane C L 2010 *Rev. Mod. Phys.* **82** 3045
[3] Ando Y 2013 *J. Phys. Soc. Jpn.* **82** 102001
[4] Chen Y L, Analytis J G, Chu J H , Liu Z K, Mo S K , Qi X L, Zhang H J, Lu D H, Dai X, Fang Z, Zhang S C, Fisher I R, Hussain Z and Shen Z X 2009 *Science* **325** 178
[5] Chen Y L, Liu Z K, Analytis J G, Chu J H, Zhang H J, Yan B H, Mo S K, Moore R G, Lu D H, Fisher I R, Zhang S C, Hussain Z and Shen Z X 2010 *Phys. Rev. Lett.* **105** 266401
[6] Sato T, Segawa K, Guo H, Sugawara K, Souma S, Takahashi T and Ando Y 2010 *Phys. Rev. Lett.* **105** 136802
[7] Zhang H, Liu C X , Qi X L , Dai X, Fang Z and Zhang S C 2009 *Nat. Phys.* **5** 438
[8] Wang Z and Zhang S C 2012 *Phys. Rev. B* **86** 165116
[9] Raghu S, Qi X L , Honerkamp C and Zhang S C 2008 *Phys. Rev. Lett.* **100** 156401
[10] Pesin D and Balents L 2010 *Nat. Phys.* **6** 376
[11] Fu L 2011 *Phys. Rev. Lett.* **106** 106802
[12] Weng H, Zhao J, Wang Z, Fang Z and Dai X 2014 *Phys. Rev. Lett.* **112** 016403
[13] Lu F, Zhao J, Weng H, Fang Z and Dai X 2013 *Phys. Rev. Lett.* **110** 096401
[14] Zhu Z H, Nicolaou A, Levy G, Butch N P, Syers P, Wang X F, Paglione J, Sawatzky G A, Elfimov I S and Damascelli A 2013 *Phys. Rev. Lett.* **111** 216402
[15] Neupane M, Alidoust N, Xu S Y, Kondo T, Ishida Y, Kim D J, Liu C, Belopolski I, Jo Y J, Chang T R, Jeng H T, Durakiewicz T, Balicas L, Lin H, Bansil A, Shin S, Fisk Z and Hasan M Z 2013 *Nat. Commun.* **4** 2991
[16] Frantzeskakis E, de Jong N, Zwartsenberg B, Huang Y K, Pan Y, Zhang X, Zhang J X, Zhang F X, Bao L H, Tegus O, Varykhalov A, de Visser A and Golden M S 2013 *Phys. Rev. X* **3** 041024
[17] Jiang J, Li S, Zhang T, Sun Z, Chen F, Ye Z R, Xu M, Ge Q Q, Tan S Y, Niu X H, Xia M, Xie B P, Li Y F, Chen X H, Wen H H and Feng D L 2013 *Nat. Commun.* **4** 3010
[18] Xu N, Shi X, Biswas P K, Matt C E, Dhaka R S, Huang Y, Plumb N C, Radović M, Dil J H, Pomjakushina E, Conder K, Amato A, Salman Z, Paul D M, Mesot J, Ding H and Shi M 2013 *Phys. Rev. B* **88** 121102
[19] Li G, Xiang Z, Yu F, Asaba T, Lawson B, Cai P, Tinsman C, Berkley A, Wolgast S, Eo Y S, Kim D J , Kurdak C, Allen J W, Sun K, Chen X H, Wang Y Y, Fisk Z and Li L 2014 *Science* **346** 1208
[20] Hatnean M C, Lees M R, Paul D M and Balakrishnan G 2013 *Sci. Rep.* **3** 3071
[21] Hlawenka P, Siemensmeyer K, Weschke E, Varykhalov A, Sánchez-Barriga J, Shitsevalova N Y, Dukhnenko A V, Filipov V B, Gabáni S, Flachbart K, Rader O and Rienks E D L 2018 *Nat. Commun.* **9** 517
[22] Xu N, Matt C E, Pomjakushina E, Dil J H, Landolt G, Ma J Z , Shi X, Dhaka R S, Plumb N C, Radovic M, Strocov V N, Kim T K, Hoesch M, Conder K, Mesot J, Ding H and Shi M 2014 arXiv:1405.0165 [cond-mat.str-el]
[23] Kang C J , Denlinger J D, Allen J W, Min C H , Reinert F, Kang B Y, Cho B K, Kang J S, Shim J H and Min B I 2016 *Phys. Rev. Lett.* **116** 116401
[24] Neupane M, Xu S Y , Alidoust N, Bian G, Kim D J, Liu C, Belopolski I, Chang T R, Jeng H T, Durakiewicz T, Lin H, Bansil A, Fisk Z and Hasan M Z 2015 *Phys. Rev. Lett.* **114** 016403
[25] Xia M, Jiang J, Ye Z R, Wang Y H, Zhang Y, Chen S D, Niu X H, Xu D F, Chen F, Chen X H, Xie B P, Zhang T and Feng D L 2015 *Sci. Rep.* **4** 5999
[26] Xiang Z, Kasahara Y, Asaba T, Lawson B, Tinsman C, Chen L, Sugimoto K, Kawaguchi S, Sato Y, Li G, Yao S, Chen Y L, Iga F, Singleton J, Matsuda Y and Li L 2018 *Science* **362** 65
[27] Bansil A, Lindroos M, Sahrakorpi S and Markiewicz R S 2005 *Phys. Rev. B* **71** 012503